BOLLETTINO DI GEOFISICA TEORICA ED APPLICATA VOL. 42, N. 3-4, PP. 183-208; SEP.-DEC. 2001

Analysis of site response in the Athens area from the 7 September 1999, Mw=5.9 Athens earthquake and aftershock recordings, and intensity observations

E. IOANNIDOU(1), N. VOULGARIS(1), I. KALOGERAS(2), L. HUTCHINGS(3) and G. STAVRAKAKIS(2)

(1) *Department of Geophysics- Geothermics, University of Athens, Greece*
(2) *Institute of Geodynamics, National Observatory of Athens, Greece*
(3) *Lawrence Livermore National Laboratory, Hazards Mitigation Center, Livermore, California*

(Received December 20, 2000; accepted April 22, 2002)

Abstract - We investigate to what extent relative damage from local earthquakes can be predicted by estimating site response or by mapping surface geology. We estimate site response in the Athens area from recordings of aftershocks of the 7 September 1999, Mw = 5.9 Athens earthquake at 22 stations. The highest damage from this earthquake was about 15 km from the epicenter. The sites studied are in and around the highest damage area and at about the same distance from the hypocenter, so that differences in site conditions may be the stronger factor in determining where damage occurred. We describe site response from weak motion recordings in two ways: 1) by an inversion to estimate site specific t_g^*, and 2) by calculating site response relative to reference sites by the spectral ratio method. We also assemble site specific information on geology of the recording sites and categorize it. We compare these results to estimated intensity at each site to evaluate whether these factors can provide an indicator of potential damage from local earthquakes. We conclude that the spectral ratio method is the best indicator of potential damage. The four sites that had the highest intensities showed the highest amplifications by the spectral ratio method, and most other sites showed relative amplifications consistent with intensity. t_g^* is a moderately effective method of identifying relative intensity, but did not identify the highest intensity area. Near-surface site geology showed very poor correlation with potential damage. Spectral ratios and t_g^* did not correlate with geology very well, but show significant correlation with each other. Microzonation mapping may be better served by mapping spectral ratios and t_g^* rather than surface geology to predict potential hazard.

Corresponding author: E. Ioannidou; Department of Geophysics - Geodynamics, University of Athens, 15783 Greece; phone: +30 22210 29276; fax: +30 22210 87519; e-mail: elioan@geol.noa.gr

1. Introduction

The 7 September 1999, Mw = 5.9 Athens earthquake is the first moderate-to-strong earthquake ever reported to have occurred at such a small distance (20 km) from the historical center of the city. Officials reported that about 100 buildings collapsed, which caused 143 casualties. The highest damage from this earthquake was about 15 km from the epicenter. The sites studied here are in and around the highest damage area and at about the same distance from the hypocenter, so that differences in site conditions may be the stronger factor in determining where damage occurred.

In this paper we investigate to what extent damage from local earthquakes can be predicted by estimating site response or by mapping surface geology. We estimate site response in the Athens area from recordings of aftershocks of the Athens earthquake at 22 stations. We also assemble site specific information on geology of the recording sites and categorize it. We describe site response from weak motion recordings in two ways: 1) by an inversion to estimate site specific t^*, and 2) by calculating site response relative to reference sites by the spectral ratio method. t^* is raised to the negative power of the exponent to model attenuation, as discussed below. We compare site response results to estimated intensity at each site in order to evaluate whether these factors can provide an indicator of potential damage from local earthquakes. If small earthquakes provide pertinent information, then they could be routinely used to provide microzonation mapping for seismic hazard mitigation. Of course, all weak motion estimates of site response only examine linear site response.

Techniques typically used to obtain site response estimates include Fourier amplitude spectral ratios of single events (Borcherdt, 1970) and averaged values from a number of events (Jarpe et al, 1989; Blakeslee and Malin, 1991) (the approach used here), cross-spectral ratios (Steidl, 1993; Safak, 1997), horizontal-to-vertical spectral ratios (Nakamura, 1989; Field and Jacob, 1993; Lermo and Chavez-Garcia, 1993; Lachet and Bard, 1994; Bonilla et al., 1997), coda spectral ratios (Aki, 1969; Malin, 1980), complex-signal spectral ratios (Steidl, 1993; Bonilla et al., 1997; Tumarkin and Archuleta, 1997), system identification (Glaser, 1995; Baise and Glaser, 2000), and forward modeling, such as with SHAKE (Schnabel et al., 1972; Idriss, 1990) and SHAKE90 (Seed et al, 1991; Rollins et al, 1994). Safak (1997) and Baise et al. (2002) summarize approaches and theory for many of these techniques. Most of these methods rely on proper input motions (reference sites) for the site response calculation. In this study, we investigate an inversion approach to obtain site response without reference sites by identifying the site specific t^*. We also use nearby reference sites to calculate spectral ratios of horizontal components in the traditional sense.

Previous studies to identify site response by inversion include Hartzell (1992) and Bonilla et al. (1997), who solved for the site term in the far-field ground motion relation. Lindley and Archuleta (1992) fit a source spectrum model and t^* to individual station spectrum with a least squares best fit. Andrews (1986) used linear least-squares inversion to solve for separate station and event spectra. He used seven events clustered together so that the individual station terms were the same for each event and simultaneously solved for the source terms of the seven events. We correct for whole path t^* and perform a simultaneous inversion by using several

stations recording the same event and fit a common Brune (1971) source spectra and site specific t^* to the observed spectra. Together, whole path and site specific t^* is essentially what Anderson and Hough (1984) call kappa.

The National Observatory of Athens, Institute of Geodynamics (NOAIG) recorded the main earthquake and aftershocks at several locations in the metropolitan area (Kalogeras and Stavrakakis, 1999), and the University of Athens, Department of Geophysics-Geothermics (UoADGG) recorded aftershocks in many locations where damage was significant (Papadimitriou et al., 2000; Voulgaris et al., 2000). Fig. 1 shows the morphology of the Athens area, the epicenter of the main shock, and locations of stations used in this study. Table 1 lists permanent NOAIG stations and temporary UoADGG stations used in this study.

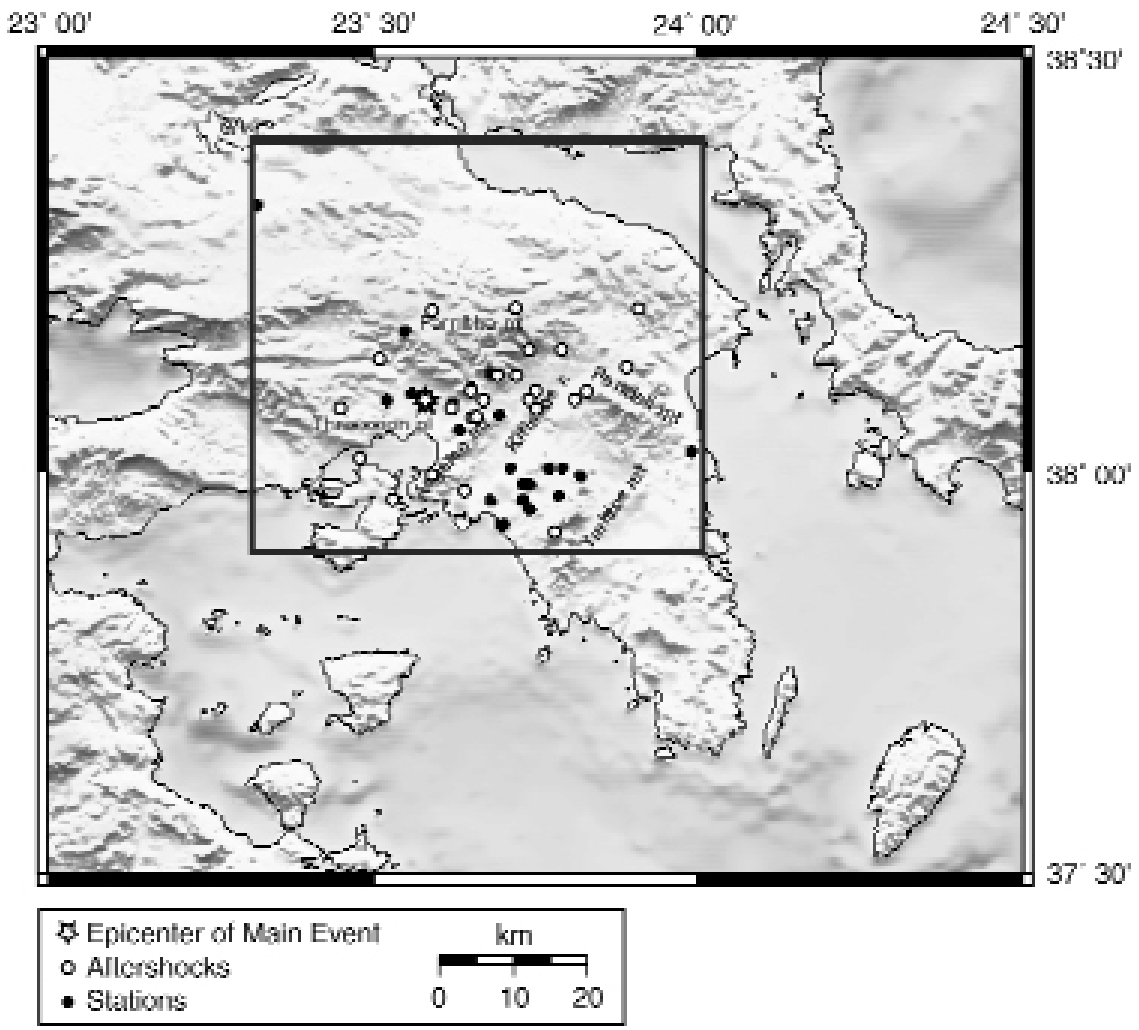

Fig. 1 - The morphology of the Athens area, the epicenter of the main shock, and locations of stations and events used in this study.

Table 1 - Stations.

Station	Latitude (N)	Longitude (E)	Location	Orientation°	No. events	Geol categ	Site specific t_g^*
ATHA+	38.00°	23.77°	Neo Psihiko;3-s reinforced concrete (RC); -13m	N180°E	16	c	.0031 ± .0002
ATHB++	37.93°	23.70°	Neo Faliro; Planetarium,3-s RC	120°	4	c	.0025 ± .0012
COUR**	38.10°	23.65°	Fili, Soccer Stadium	0°	5	a	.0027 ± .0008
DEKL++	38.10°	23.78°	Dekelia, Air Base, 1-story	175°*+	4	c	.0271 ± .0097
DFNA+	37.95°	23.74°	Dafni; Metro station, -14m	155°*+	1	c	.0086 ± ---
DMKA+	37.99°	23.82°	Ag.Paraskevi; Research center, 1-story RC	135°	4	b	.0024 ± ---
FIXA+	37.96°	23.73°	Sygrou-Fix; Metro station, -15 m	140°	4	c	.0046 ± ---
PEFK**	38.08°	23.62°	Thriassion plain, Ware House 1-story	0°	6	c	.0037 ± .0014
PNTA+	38.00°	23.79°	Papagos; Metro station, -15m	135°	1	c	.0067 ± ---
RFNA+	38.02°	23.99°	Private building, 1-s wood	250°*+	1	b	.0048 ± ---
RNTA++	37.96°	23.68°	Rentis; Town Hall, 2-s RC	210°	3	c	.0075 ± ---
SGMA+	37.98°	23.74°	Syntagma; Metro station,-7m	010°	7	b	.0051 ± .0014
SGMB+	37.98°	23.74°	Syntagma; Metro station, -26m	135°	3	b	.0076 ± ---
SPLA+	38.00°	23.71°	Sepolia; Metro station, -13m	320°	18	c	.0053 ± .0017
SPLB+	38.00°	23.71°	Sepolia; Metro station, 3-s steel	320°	19	c	.0046 ± .0021
FILI**	38.12°	23.68°	Fili Monastery, free field	0°!	6	b	.0034 ± .0015
THVC+	38.32°	23.32°	Thiva; Town Hall, 3-s RC	180°	5	b	.0027 ± .0016
PSAR**	38.09°	23.56°	Goritsa, house, ground fl, RC	0°	6	c	.0166 ± .0010
MAGO**	38.08°	23.52°	Magoula, 1-story RC	0°!	6	a	.0056 ± .0019
STEF** N00E bad	38.17°	23.55°	Stefani, Storage, ground fl, RC	0°!	5	b	.0111 ± .0032
ZOFR**	38.07°	23.69°	Zofria; free field	0°	6	a	.0026 ± .0011
NEOK**	38.05°	23.63°	Neokista ground fl, RC	0°!	6	a	.0024 ± .0007

° Orientation of the longitudinal component (l). The orientation of the transverse component (t) is: t = l + 90°
+ NOAIG station
++ NOAIG, did not record main event
** Univ. of Athens data, did not record main event
*+ t component -90.0 from l component
! polarity may be reversed

2. Geology

The neotectonics of greater Attica area consists of a complex post-alpine structure, which is characterized by complicated kinematic and dynamic evolution and involves major fault blocks with different rotational axes trending NE-SW and E-W. This structure consists primarily of the tectonic graben of Thriassion plain and the complex neotectonic graben of West Athens basin; the mountains of Parnitha and Aegaleo belonging to the Mesozoic non-metamorphic Eastern Greece unit; and the Pendeli and Ymittos mountains belonging to the Mesozoic metamorphic unit. The tectonic contact of these units is interpreted to be in the NE-SW direction with its location coinciding with the Kifissos River (Mariolakos and Foundoulis, 2000); this roughly coincides with the Miocene thrust feature shown in Fig. 2. The epicentral area of the Athens

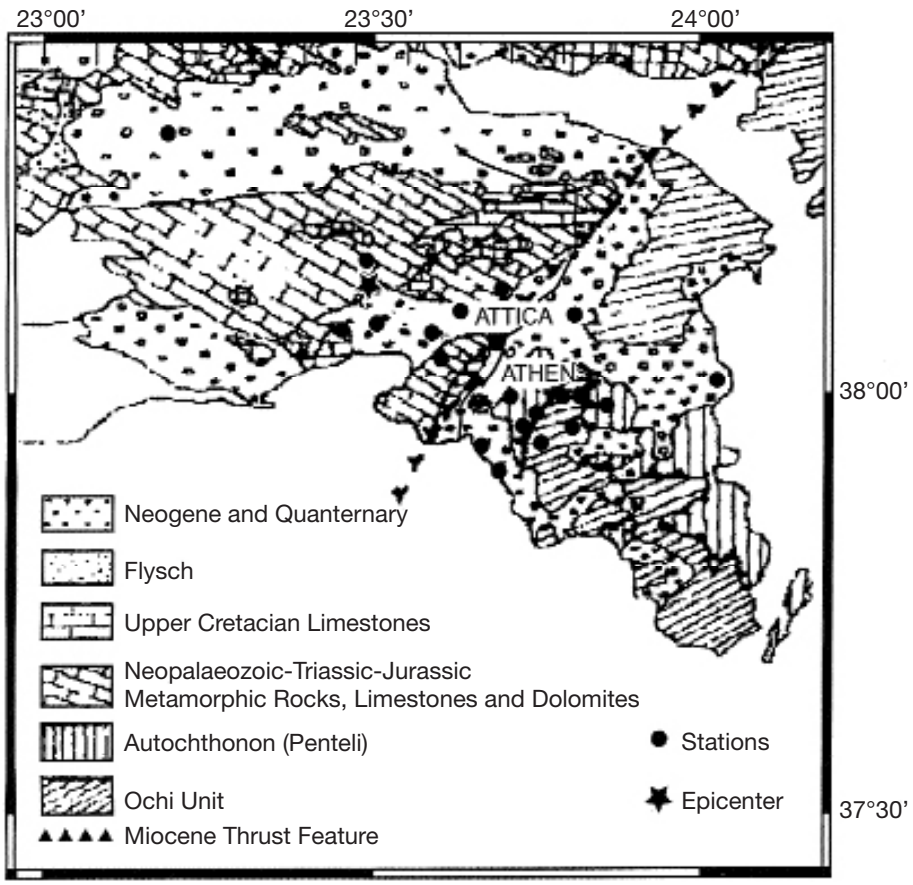

Fig. 2 - Geology of the lower border area of Attica (modified from Katsikatsos et al., 1986), station locations, and epicenter of main event.

earthquake is situated near the proposed boundary of the two units but the absence of detailed geological mapping does not allow determination of their tectonic relation (Mariolakos and Foundoulis, 2000). Fig. 2 shows the geology of the study area and the recording sites and major tectonic features; the epicenter is shown by a star. From Figs. 2 and 3, it may be observed that the majority of the recording sites, except that from Thiva (THVC), lay on the hanging wall, to the east, of the probable N113°E fault orientation for the 1999 Athens earthquake (Ioannidou et al., 2002).

Table 2 describes the geology of the recording sites. The geology of the sites is primarily shales, sandstones, crystalline limestones, and soil conditions from firm soil to alluvium. Most of the recording sites lay in the vicinity of major infrastructure, having been constructed in the past or being under construction at the time of the earthquake, i.e. the surface or underground stations of the Athens Subway (DFNA, FIXA, PNTA, SGMA, SGMB, SPLA, SPLB). Hence, it has been possible to collect data from previous geotechnical investigations and describe the local ground conditions at the recording sites. Table 2 also lists categories of geologic site conditions. According to Bouckovalas et al. (2002) the sites were classified into two categories taking into account the peak of the Normalized Horizontal-to-Vertical Spectral Ratio

Table 2 - Geology of recording sites.

Site	Categ.	Geology	Dist. (km)	Intensity*
ATHA	(c)	Tertiary deposits. 0-2 m fill material, 2-6 m poorly cemented conglomerate, 6-20 m very weathered sandstone, 20-30 m sandstone (Attiko Metro, 1999)	25	V+, Filothei
ATHB	(c)	Holocene deposits. 0-1m soil, 1-8 m brown sandy clay with pebbles, 8-12m brown stiff sandy clay, 12-20 m brown stiff clay (Geomechaniki Ltd., 1999)	25	V+, Alimos; VI, Ag. Dimitrios
COUR	(a)	Middle Triassic - Lower Jurassic (Mesozoic). Dolomite-limestone formation, considerably fractured and folded. In the station area this formation overlies the Permian formation with a maximum thickness of 50 m	18	VIII**
DEKL	(c)	Recent Deposits	24	VIII**
DFNA	(c)	Alluvium schist; 0-3.5 m alluvial deposits, 3.5-9 m Athenian schist - sandstone medium weathered, 9-30 m Athenian schist - sandstone slightly weathered (Attiko Metro, 1999)	26	V+, Agios and Dimitrios
DMKA	(b)	0-1 m fill materials, 1-3 m conglomerate altered to clayey sand gravel, 3-4 m brown schist with many cracks and calcareous veins, 4-12 m very humified peridoite, altered locally to clayey - loose or synectic - sand gravels. The site according to the New Seismic Resistant Code could be characterized as very altered rock sites, which are classified as granular soils from the engineering point of view (Tsamis, 1999)	29	V+, Vyronas
FIXA	(c)	Alluvium schist; 0-2 m fill materials, 2-6.5 m Athenian schist - calcareous siltstone, 6.5 11 m Athenian schist - quartzy siltstone, 11-14.5 m siltstone and lime stone, 14.5-30 m siltstone, calcareous siltstone and quartzy siltstone (Attiko Metro, 1999)	25	VII**
PEFK	(c)	Quaternary deposits	17	VII**
PNTA	(c)	Tertiary deposits; 0-3 m fill material, 3-20 m slightly cemented silty clay, 20-29 m shales (Attiko Metro, 1999)	26	V+, Filothei
RFNA	(b)	Tertiary deposits limestone	40	V, Lavrio; Keratea V+
RNTA	(c)	Alluvium schist; 0-1.5 m soil, 1.5-4 m sandy siltstone, 4-7.5 m brown clay, 7.5-13 m mixture of sand, clay and silt, 13-15.5 m sand, 15.5-20 m sand and gravels, 20-23.5 m stiff marl (PWRC, 1981)	23	VI
SGMA	(b)	Schist; 0-12 m Athenian schist - sandstone slightly weathered, 12-28 m Athenian schist - sandstone slightly weathered and fractured (Attiko Metro, 1999)	25	V+
SGMB	(b)	Schist; 0-12 m Athenian schist - sandstone slightly weathered, 12-28 m Athenian schist - sandstone slightly weathered and fractured (Attiko Metro, 1999)	25	V+
SPLA	(c)	Alluvium schist; 0-6.5 m fill material, 6.5-13.5 m slightly cemented silty clay, 13.5-17 m strongly cemented conglomerate, 17-22.5 m sandy siltstone, 22.5-24 m calcareous siltstone (Attiko Metro, 1999)	22	VII
SPLB	(c)	Manmade deposits; 0-6.5 m fill material, 6.5-13.5 m slightly cemented silty clay, 13.5-17 m strongly cemented conglomerate, 17-22.5 m sandy siltstone, 22.5-24 m calcareous siltstone (Attiko Metro, 1999)	22	VII
FILI	(b)	Schist; Upper Palaeozoic (Permian). This formation consists of alterations of phyllites, sandstones, shales and graywackes, which appear significantly fractured folded and weathered, resulting to the existence of soil cover of important thickness. Due to the long history of tectonic deformation in the area, this formation is overthrusted on the Triassic-Jurassic limestone formation	19	VIII, Fili

Table 2 - continued.

THVC	(b)	Pleistocene deposits; 0-2 m slightly cemented silty clay, 2-4 m poorly cemented conglomerate, 4-6 m strongly cemented conglomerate, 6-24 m conglomerate (limestone pebbles in a reddish silty clay) (Edafomechaniki Ltd., 1998)	39	V, Thespies; V, Akrefinio; IV, Istiaia
PSAR	(c)	Neogene-Quaternary; Plioquaternary deposits of considerable depth, which mainly represents the product of erosion from the surrounding geological formations. Due to the unconsolidated nature and the sandy and silty character of these deposits this area can be characterized as a "soft" site"	17	VII**
MAGO	(a)	Limestone, Upper Cretaceous Limestone, uncomfortably overlies the dolomites and limestones of Mi-Triassic - Lower Jurassic	18	VII**
STEF	(b)	Schist; Upper Palaeozoic (Permian). This formation consists of alterations of phyllites, sandstones, shales and graywackes, which appear significantly fractured folded and weathered, resulting to the existence of soil cover of important thickness. Due to the long history of tectonic deformation in the area, this formation is overthrusted on the Triassic-Jurassic limestone formation	20	VII**
ZOFR	(a)	Limestone, Middle Triassic - Lower Jurassic (Mesozoic). Dolomite-limestone formation, considerably fractured and folded. In the station area this formation overlies the Permian formation with a maximum thickness of 50 m	19	VIII**
NEOK	(a)	Limestone; Lower Jurassic (Mesozoic). Dolomite-limestone formation, considerably fractured and folded	18	VII**

* Intensities on the Modified Mercalli Scale calculated by the NOGIA for the main event (Kalogeras and Stavrakakis, 1999), and names of districts near the station where the intensity was evaluated.

** Intensity values interpreted from isoseismals in Fig. 3.

(ANHVSR), the fundamental period of the Normalized Horizontal-to-Vertical Spectral Ratio (TNHVSR) and the ratio of peak ground velocity over peak ground acceleration (vmax/amax). We have added an additional category for hard rock sites:

1. Hard rock formations. Dolomites or limestone of U. Triassic to L. Jurassic age and limestone of U. Cretaceous age. A small difference should be expected between these two members of this group mainly due to the higher tectonic deformation associated with the older group.
2. Rock - Soft Rock formations. It includes all sites with ANHVSR less than 3, vmax/amax ratio less than 60 cm/s/g and corresponding site periods TNHVSR between 0.07 and 0.26 s. The geological formations belonging to this category are slightly to medium weathered phases of the Athens Schist, metamorphosed schist and limestone, cohesive talus cones and medium to well cemented conglomerates or neogene marls.
3. Soil - Stiff Soil formations. It includes the remaining sites with ANHVSR over 3, vmax/amax ratio over 60 cm/s/g and corresponding site periods TNHVSR between 0.22 and 0.50 s. In geological terms, the formations of this category include moderately thick weathering products of the geological bedrock, alluvium deposits of medium to high density or recent manmade deposits. Moreover, the layer thickness of the softer material of category (c) is expected to represent an important factor in the observed site response due to energy diffusion over a wider band of the spectrum.

3. Intensity and damage to engineering structures

Fig. 3 shows the isoseismal intensity from the earthquake as it has been compiled after Protonotarios (1999) in Modified Mercalli Scale (MMS). This map is consistent with the individual MMS values determined in the vicinity of most NOA stations (Kalogeras and Stavrakakis, 1999). These individual values are listed in Table 2, along with the names of districts near the station where the intensity was evaluated. If no individual values are available for a site, then we used the isoseismal map in Fig. 3 to estimate the intensity. Other researchers have determined high intensity values in a mezoseismal area that covers the area encircled by the IX isoseismals in Fig. 3. This includes the districts of Ano Liosia, Menidi, Metamorphosi, and Adames. These researchers use the European Macroseismic Scale 1998 (EMS-98), which considers additional criteria than the MMS, but the estimated intensities in EMS-98 are about

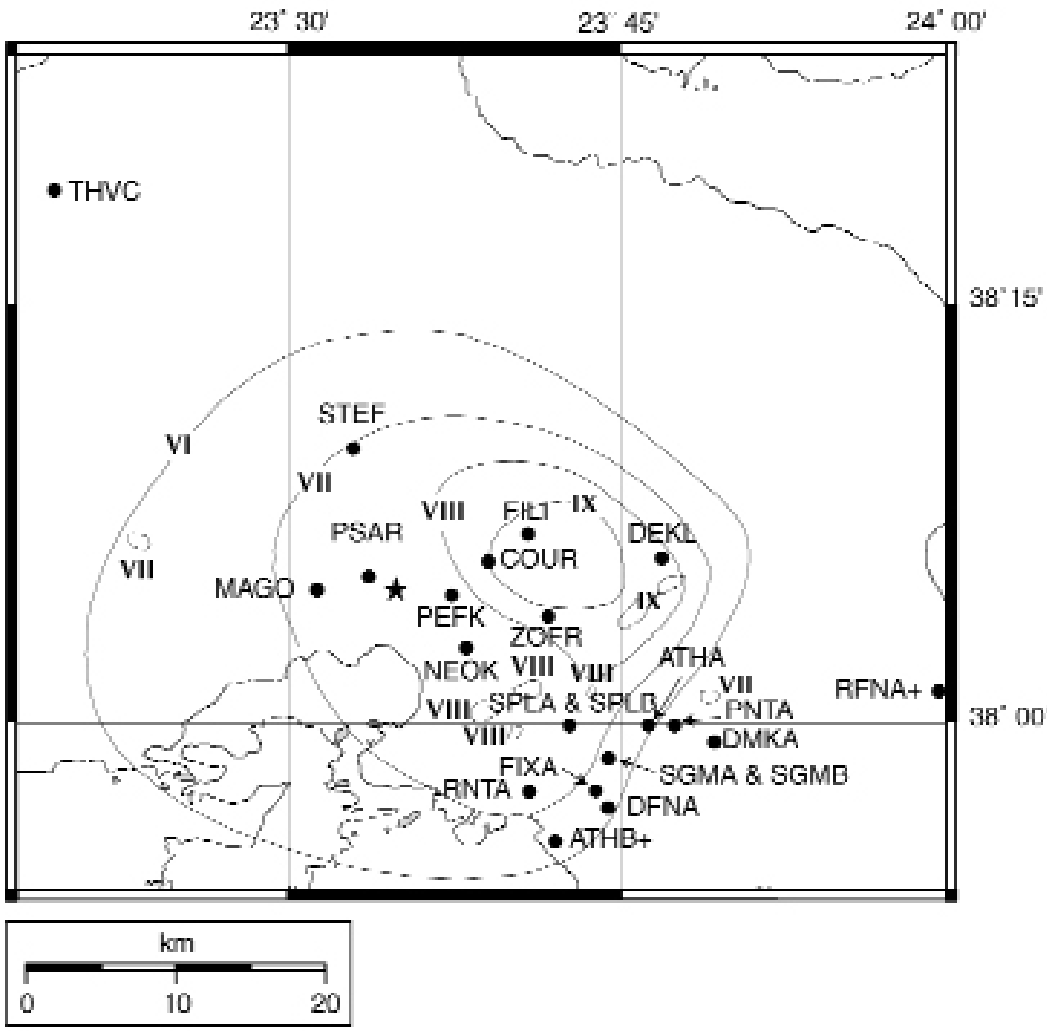

Fig. 3 - Isoseismal intensity from the earthquake in Modified Mercalli Scale, and individual intensity values for the same area as specified in Table 2.

equivalent to MMS values for the range of values used in this study. Kouskouna et al (2000) estimate values of IEMS-98 = VIII-IX and Lekkas (2001) maps values of IEMS-98 = IX and IEMS-98 = X in the aforementioned districts, where many weaker structures collapsed and heavy damage occurred in reinforced structures. Intensities values IEMS-98 = VIII, VII surround these areas forming elongated contours that extend southward in the NNE - SSW direction, while values IEMS-98 = VII are also reported, in specific locations of Elefsina and Aspropyrgos, south of the epicenter and at Chalandri and Dafni to the east of the epicenter (Kouskouna et al., 2000, Lekkas, 2001).

Most of the damage occurred within an area of 10 km mostly northeast of the epicenter. Severe damage decreased rapidly with the distance from the center of high isoseismals, while in most areas of Athens damage was non-structural and consisted, mainly, of cracks to in-fill brick walls. The distribution of damage is not typical and may have been affected by the site conditions. Insufficient construction foundations and/or the local topography seem to play a significant role in the partial or total collapse suffered by a number of industrial buildings along the west bank of the Kifissos River. Interpretation of the isoseismal map may be affected by the location accuracy of the earthquake. However, due to its depth, the travel distance to the sites of interest will not change significantly with small changes in the earthquake location, although the Athens earthquake was a moderate event. It is worth, to note that projection up-dip of the proposed fault plane intersects near the high damage area.

A special report published, electronically, by EERI (1999) a few days after the main shock, describes damage in detail. An outline of this description reports: All classical monuments survived the earthquake almost without damage and only minor effects were reported in some cases. Small rotations of some columns and the fall of small pieces of marble were reported for the Acropolis of Athens, but were considered of minor importance by the archaeologists. Historical masonry buildings of the last century did not suffer significant damage (National Archaeological Museum, Iliou Melathron, Byzantine Museum, and Metropolitan Church). Older monuments which were already in bad condition sustained significant damage (Moni Dafniou, a Byzantine monastery of the 11th century).

No damage was reported on highways, roads or railroad tracks, except for cracks and minor landslides on the road leading to the summit of Parnitha mountain, near the epicenter. Underground pipelines behaved well. The recently constructed natural gas network did not suffer any damage at all, although it crosses the mezoseismal area at a shallow depth. No damage was reported to the new underground metropolitan railway. The Mornos duct way, which supply Athens, suffered no damage, although it runs almost parallel to the Aspropyrgos fault and through the mezoseismal area.

4. Data

NOAIG manages data recorded by their permanent strong motion array and the Attico Metro S. A. instruments. Stations DFNA, RFNA, MNSA, DEKL are analog SMA-1 Kinemetrics electromagnetic type recorders, and the other Observatory stations are Teledyne-Geotech,

12 bit resolution with tri-axial force balance seismometers. The procedure for processing strong motion records of NOAIG is based on the standard procedure of the CALTECH Institute (Trifunac and Lee, 1973), and is described, in detail, by Stavrakakis et al. (1993). The instrument correction used is that described by many investigators (Hudson and Brady, 1971; Trifunac and Lee, 1973; Trifunac et al., 1973; Hudson, 1979; Trifunac and Lee, 1979), while values of Ormsby filters proposed by Basili and Brady (1978) and used by previous authors for processing strong motion records in Greece (Carydis et al., 1984; Anagnostopoulos et al., 1986; Margaris, 1986; Carydis et al., 1989; Makropoulos et al., 1989; Lekidis et al., 1991), are applied.

The UoADGG deployed two types of stations during the installation of the temporary network (Voulgaris et al., 2000). Acceleration was recorded at sites PEFK and COUR, situated within the center of the network, using Kinemetrics ETNA instruments. The previously mentioned procedure for processing strong motion accelerometer records was applied on the data from these stations. At the NEOK, STEF, MAGO, FILI, PSAR and ZOFR sites RefTek recording instruments were installed. The first four of these were equipped with the LE-3D 1 Hz Lennartz sensor while the last two stations were connected to GURALP CMG 40-T broadband seismometers. The records obtained were instrument response corrected according to the sensor specifications to obtained velocity time histories.

Table 3 lists source information for the events used in this study, including Mo and fc calculated in this study. Hypocentral locations for the main event and many of the aftershocks were obtained from Papadopoulos et al. (2000) (indicated by an * in Table 3). Locations for the events shortly after the main event (indicated by a $^{+}$ in Table 3), which were not recorded by temporary local networks, were obtained using information from the permanent networks in Greece and s-p arrival time intervals from the strong ground motion records (Kalogeras and Stavrakakis, 1999). Focal mechanism solutions were obtained from Papadopoulos et al. (2000). In addition, several events were located and focal mechanism solutions were obtained by combining data from NOAIG with that from the UoADGG. These are identified by $^{++}$ in Table 3. These hypocentral solutions are consistent with other solutions obtained in this study. Since these solutions used a different station distribution, and a slightly varied velocity model, this gives confidence that the locations of events used in this study are near the limit of accuracy that can be achieved for this area. The focal mechanism solutions from the combined data are close to that of the main event, as are many of the events listed in Table 3 from Papadopoulos et al. (2000).

5. Moment, corner frequency, and site response of events

We conducted a simultaneous inversion for source moment and corner frequency, and individual station's t^* using the computer program NetMoment (Hutchings, 2002). The joint inversion is based upon the assumption that corrected long period spectral levels and the source corner frequencies from a particular earthquake will have the same value at each site, so that differences in spectra are due to propagation path and individual site t^*. t^* is $R / (QV)$ and is

Table 3 - Events used in the study.

Earthquake	Latitude	Longitude	Depth (km)	Ml	$Mo \times 10^{20}$ (dyne-cm)	f_c (Hz)	mechanism STK	DP	SV	N. of stations°
1999/09/07 11:56:51*	38.08	23.58	16.8	5.4	94900	0.45	113°	39°	-90°**	10
1999/09/07 11:59:10+	38.15	23.59	5.0**	***	228	3				6
1999/09/07 12:00:29+	37.92	23.78	17.8	***	176	2				6
1999/09/07 12:01:57+	38.07	23.75	5.0**	***	28.5	3				2
1999/09/07 12:03:54+	38.01	23.47	5.2	3.5!	73!	6				1
1999/09/07 12:05:12+	38.11	23.69	5.0**	***	228	2				4
1999/09/07 12:08:11+	37.82	23.71	5.0**	***	269	4				4
1999/09/07 12:16:10+	37.96	23.76	17.0	***	328	4				4
1999/09/07 12:20:25+	38.09	23.65	5.0**	***	344	5				1
1999/09/07 13:02:02+	38.07	23.62	5.0	***	26.3	4				2
1999/09/07 13:05:48+	38.13	23.51	18.2	***	322	3				1
1999/09/07 15:35:33*+	38.01	23.48	10.0	3.9	150	3				6
1999/09/07 15:42:52*+	38.07	23.45	3.0	3.5	72.8	6				1
1999/09/07 17:19:21*	38.11	23.72	16.2	3.8	260	3	114°	30°	-87°	4
1999/09/07 20:44:55*	38.19	23.72	21.0	4.4	611	2				3
1999/09/08 03:21:32*	38.09	23.83	14.1	3.7	313	3				7
1999/09/08 03:35:20*	38.12	23.89	13.0	3.7	487	5	106°	30°	-74°	3
1999/09/08 11:14:29*+	37.99	23.59	7.0	3.1	46.5	3				2
1999/09/08 12:55:01*	38.14	23.74	19.9	4.0	965	2	330°	70°	-30°	2
1999/09/08 13:18:21*	38.08	23.81	9.2	3.7	99.8	3				4
1999/09/08 16:50:37*	38.19	23.91	1.4	3.6	185	4	113°	28°	-67°	1
1999/09/08 16:54:08*	38.14	23.79	19.4	3.5	350	3	310°	50°	-20°	1
1999/09/10 14:49:57++	38.08	23.67	9.1	3.7	444	3	319°	70°	-79°	10
1999/09/13 19:45:15++	38.06	23.65	9.1	3.1	95.1	3	109°	50°	-74°	11
1999/09/16 08:12:10++	38.06	23.66	7.9	3.1	93.5	3	120°	54°	-89°	11
1999/09/20 19:58:09*+	37.96	23.53	7.0	2.9	22.2	3				10
1999/09/20 20:17:25++	37.97	23.64	8.8	2.9	2.90	7	250°	65°	-48°	8
1999/10/03 17:03:34++	38.09	23.75	9.0	3.5	252	3	159°	65°	-48°	10
2000/03/23 03:09:18*+	38.08	23.74	15.0	3.5	412	3	120°	54°	-89°	4

° Number of stations which recorded the event
* Location from Papadopoulos et al. (2000)
\+ Location obtained from permanent networks in Greece and s-p arrival time intervals
++ Solution from combined data of Univ. of Athens and National Observatory of Athens
*+ Locations routinely calculated by NOAIG from their permanent Greek network
** Depth fixed
*** Magnitude obtained from moment/magnitude relationship
! Moment and magnitude obtained from spectral overlay with event 1999/09/07 15:42:52

raised to the negative power of the exponent to model attenuation as $\exp(-\pi f t^*)$. R is distance traveled, V is velocity, and Q is the seismic quality factor. We corrected spectra for whole path t_r^* and solved for site specific t_g^*. Anderson and Hough (1984) showed that to a first approximation attenuation could be separated into a near-surface attenuation and an attenuation at depth. Our assumption is that whole path attenuation is fairly uniform and determined from the velocity model. We also assume that VQ near a site will vary with individual site conditions. It is well known, for example, that poorly consolidated materials have low velocities and low Q values, and thus would have high t_g^* values. Similarly, rock has high velocity and high Q values and would have low t_g^* values. Of course, we cannot identify what is specifically contributing to t_g^*

and over what distance range. In particular, there is a trade-off between t_r^* and t_g^*. Here, we use t_r^* to normalize for propagation distance and examine relative values of t_g^*. We assume that to a first order Q and thus t^* is frequency independent. This is supported by observations to calculate Q in the shallow crust (Hough et al., 1988; Frankel and Wennerberg, 1989).

We used a nonlinear least squares best fit of displacement spectra of the S-wave energy of the recorded seismograms to the Brune (1971) source model to solve for our free parameters. The Fourier amplitude spectra of recorded seismograms were corrected to represent moment at the long period asymtote and for whole path attenuation. They were then fit to the Brune displacement spectral shape with site specific t^* and moment as the long period spectral asymtote. Spectra were fit to the modified Brune spectra:

$$\Omega(f) = \frac{M_0 \exp(-\pi f t_g^*)}{\left[1 + \left(\frac{f}{f_c}\right)^2\right]} \tag{1}$$

where M_0 is the moment, f is frequency, f_c is the source corner frequency, and t_g^* is site specific t^*. The best fitting combination of free parameters (M_0, f_c, t_g^*) was found by iteration from a starting model using the Simplex algorithm (Nelder and Mead, 1965; Caceci and Cacheris, 1984; Press et al., 1998). Units are dyne-cm.

The correction to spectra prior to the joint inversion is based upon the equation for moment from Aki and Richards (1980). Spectra of recorded seismograms were corrected by:

$$\Omega'(f) = \frac{4 \pi R \rho_x^{1/2} \rho_\xi^{1/2} \beta_x^{1/2} \beta_\xi^{5/2}}{S^S F^S} U(f) \exp(\pi f t_r^*) \tag{2}$$

where $U(f)$ is the recorded displacement spectra, t_r^* is whole path t^*, R is correction for geometrical spreading, ρ_x is density at the station and ρ_ξ is density at the source, β_x is shear velocity at the station and β_ξ is shear velocity at the source. S and F are the free surface correction and focal mechanism correction, respectively. The free surface correction is determined from the velocity model using the reflection coefficients as outlined in Aki and Richards (1980). The focal mechanism correction is determined by the radiation pattern as outlined by Aki and Richards (1980), and discussed further below. Density is determined from the shear wave velocity by the linear relation: $\rho = (\beta - 0.35) / 1.88$ (Lama and Vutukuri, 1978). Then, the seismic moment M_0 is determined by $\Omega'(f \rightarrow 0) = M_0$.

Ten seconds of S arrivals were used in the calculation. We are using Q_s for whole path t^* since only S-waves are used in the inversion. Seismograms were rotated to radial and transverse components, and the vertical and radial were square-of-sum-squared added to get one Sv spectrum, then the Sv and Sh components were corrected for focal mechanism solution. Sv and Sh components were square-of-sum-squared added to get one S-wave spectrum and corrected with the remaining corrections of Eq. (2) before the inversion. Corrected spectra were fit to equation 1 by fitting frequencies from 1.0 to 20.0 Hz for most aftershocks, and 0.3 to 25.0 Hz for the main event. Some aftershocks had better signal to noise and were fit to 0.5 to 20.0 Hz,

and some had worse signal to noise and were fit to 2.0 to 15.0 Hz. These frequency ranges ensured that all recordings were above noise. Table 3 lists the number of aftershocks recorded at each station and used in the inversion.

Obviously, model parameters are dependent upon the constants used in the Eqs. (1) and (2). We attempted to identify the uncertainty attributed to these constraints. The moment is dependent upon shear velocity to the 4^{th} power, since shear velocity is to the 3^{rd} power in Eq. (2) and density is determined from the shear velocity from the linear relation: $\rho = (\beta - 0.35) / 1.88$ (Lama and Vutukuri, 1978). In Eq. (2): $\rho_x = 2.37$ g/cm^3 is the surface density and is based upon near-surface basement rock P-wave velocity of 4.1 km/s. It is assumed that the long period waves used to calculate moment sample primarily the basement structure. ρ_ζ varies with the depth of the event, $\rho_\zeta = 3.26$ g/cm^3 for the main shock. A difference of 20% in shear velocity results in a change in moment value of about a factor of 2.

There is a fairly significant scatter in long period spectral levels of a factor of up to ± 5. This may be due to either a difference in site response at low frequencies, an inappropriate correction for focal mechanism solution, directivity effects, hypocentral location, or unidentified long period noise. We excluded significant directivity effects as the cause because of the size of aftershocks used, and determined that at frequencies between 1.0 and 20.0 the signal to noise ratio was such that noise was not a cause. We also identified that a similar difference in spectral amplitudes as observed at long period spectral levels was evident throughout the frequency range of recording. This suggests that it is due to inappropriate focal mechanism solution (FMS) corrections or systematic amplifications. We examined the effect of FMS correction for amplitude and found that there was a reduction in the scatter if a FMS correction was applied. If a FMS was available, we applied a correction that was limited to a minimum of 0.25 (see Hutchings and Wu, 1990). If a FMS was not available, an average value of 0.63 was used for the FMS radiation pattern correction (Wu and Ben-Menahem, 1965). We could not identify whether site response was a contributing factor. We calculated the standard deviation of the moment calculation for all the events together to be a factor of ± 2.1.

The fit to t_g^* and *fc* are dependent upon the long period spectral level and in a simultaneous inversion this can result in a bias. For example, if a site has a factor of 2 greater long period spectral level than the solution for the joint inversion, and is forced to fit the site specific high frequency, then the t_g^* value will be higher and the f_c will be lower than if spectra were fit individually. Therefore, in an effort to get unbiased value of t_g^* and f_c we normalized spectra to have the same long period spectral level (average of all recordings for a particular event), then conducted the simultaneous inversion. This did not affect the moment calculation significantly because t_g^* generally has minimal effect at these periods and the spectral fit of the inversion is primarily the mean of long period values anyway. This inherently adds the assumption that at the longest periods, site response is not a factor.

There is an obvious trade-off between the t_r^* correction and t_g^*. However, we found essentially no trade-off between source corner frequency and choice of Q_s between 250 and 1000 for t_r^*. We have limited the range for whole path Q_s of between 250 and 500 from previous studies of Q_s and our analysis. Hashida et al. (1988) used macroseismic data and found that an average Q_s ranges between 50 and 1000 for the crust for the whole area of Greece and that the

Continental Greece is an area of higher Q_s in the crust than the Aegean area. Papazachos (1992) by using the same kind of data but in a different approach estimated a mean Q_s of 350 ± 140 at around 1 Hz for the same region. Hatzidimitriou et al. (1993) by using acceleration data found Q_s values ranging between 30 and 360 for frequencies 4-10 Hz. We found that a Q_s value of 350 to 500 for whole path Q correction gave the most consistent spectral fall-off at all stations. In particular, lower values of Q_s resulted in an over correction when applied to distant stations, such as THVC and RFNA, and a spectral slope that was lower at higher frequencies. We have used a value of $Q_s = 350$ for t_r^* correction.

Table 1 lists individual t_g^* values obtained from program NetMoment, along with one standard deviation values of those sites that had 4 or more recordings. Table 3 lists the moment and corner frequency obtained for the source events. A reliable moment value was not obtained for the main event because the source corner frequency is near the low frequency recording limit of about 0.5 Hz. Fig. 4 shows a plot of calculated t_g^* values at each station. The circle size

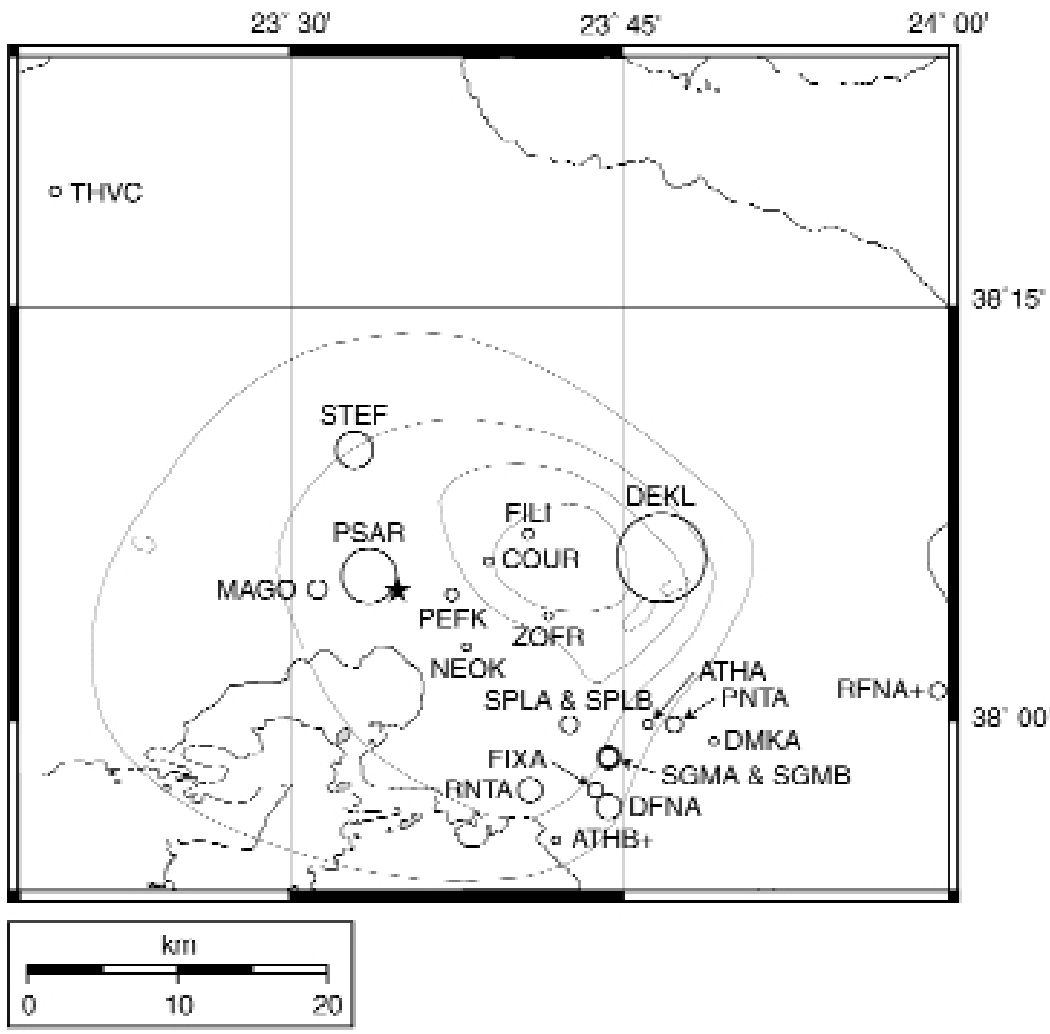

Fig. 4 - Plot of calculated site specific t_g^* values at each station. The circle size corresponds to t_g^* values.

corresponds to t_g^* values. Figs. 5 and 6 show fits of moment, the Brune source model, and t_g^* to corrected spectra for twelve of the events. There are several points that should be noted. First, there is one spectral fit for each spectra plotted, and they all converge to a common asymptotic value, the moment. The spectra are shown only for the frequency range where data is considered adequate for the study, and the asymptotic fit to the Brune source model may have a higher value than is indicated by the plot. Since t^* is not allowed to be negative, spectra that have a slope less than the $1/f^2$ of the Brune source model cannot be fit. See, for example, the spectra with shallow slope for event 990907115651, the main event. Spectra such as these will have t_g^* of zero, and are interpreted to have had no t_g^*. It is recognized that a site specific amplification can have this effect, and thus bias results. Generally, spectra show varying slopes of the high frequency fall-off due to t_g^*.

Fig. 7 shows the corner frequency values as a function of moment for the events in this study. Also plotted is the corner frequency relationship predicted by a Brune source model with

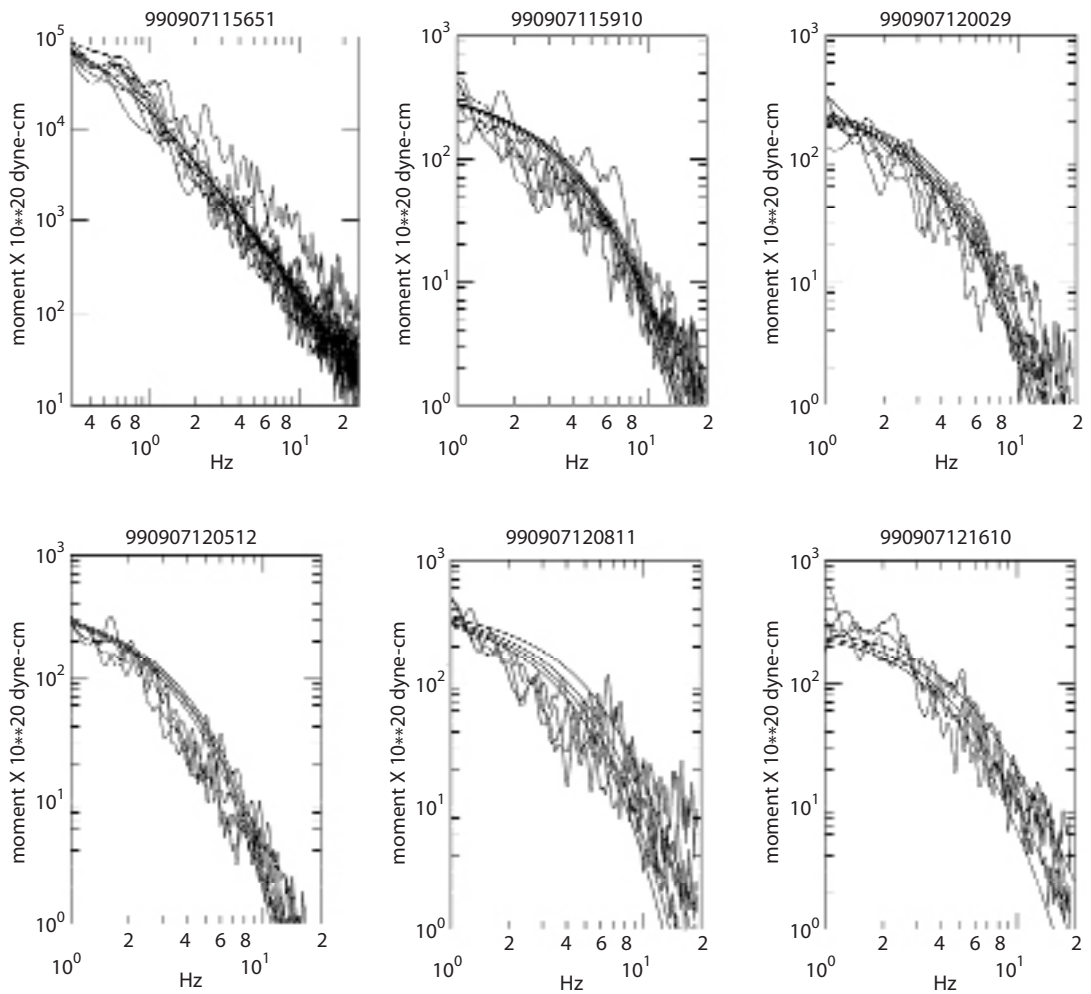

Fig. 5 - Corrected spectra, as described in text, of all recordings for six events, and the fit of the simultaneous inversion for moment, source corner frequency, and individual station t_g^*.

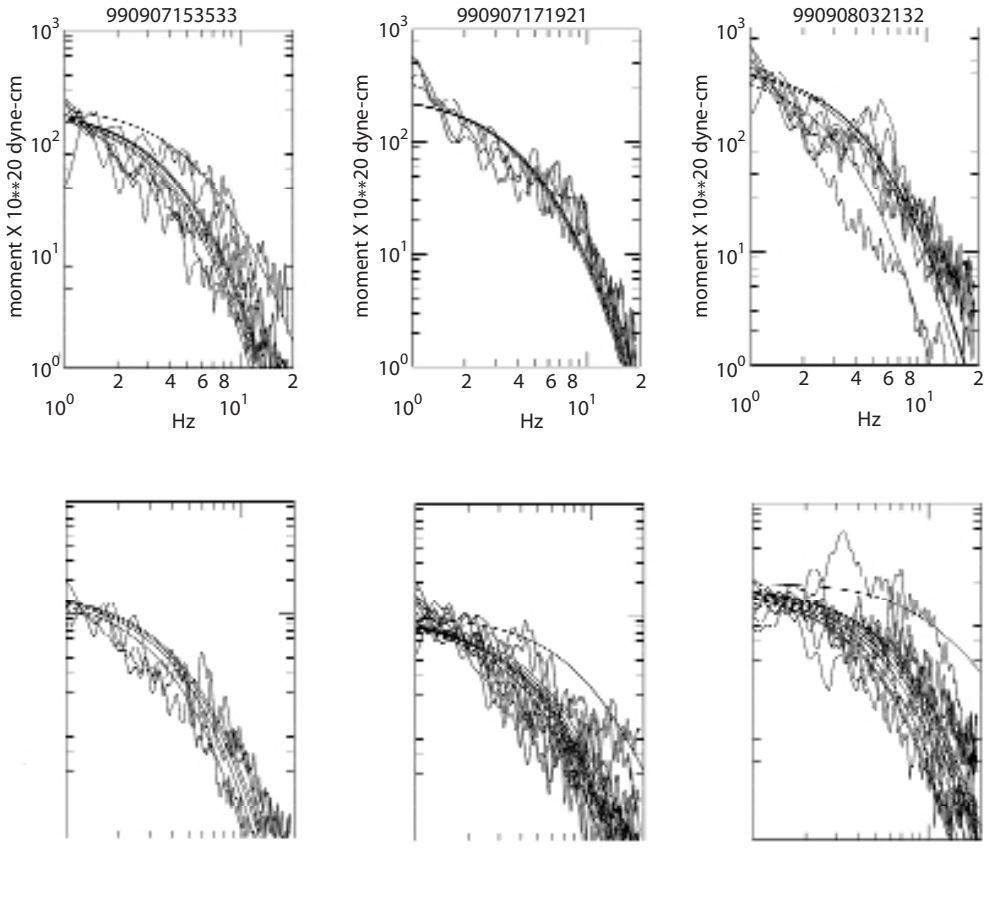

Fig. 6 - Corrected spectra, as described in text, of all recordings for six events, and the fit of the simultaneous inversion for moment, source corner frequency, and individual station t_s^*.

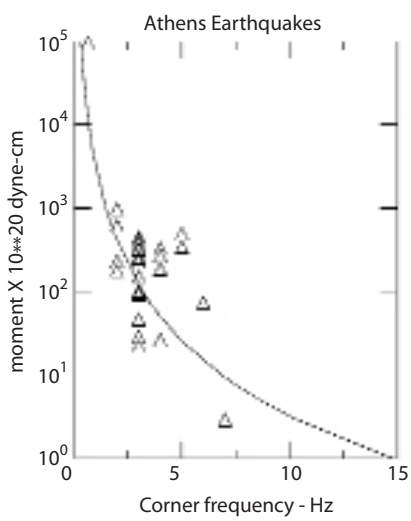

Fig. 7 - Corner frequency values as a function of moment for the events in this study (triangles) and the corner frequency relationship predicted by a Brune source model with 100 bar stress drop (solid line).

100 bar stress drop. It is apparent that corner frequencies identified in this study are consistent with those generally described by the Brune source model. Scatter in corner frequencies may be due to variation in stress drop or uncertainties in corner frequency picks. Trial and error calculations for this study shows that corner frequency picks vary by about ± 1 Hz, depending upon choices in calculating the L_2 norm.

6. Spectral ratios

Spectral ratios were obtained for clusters of stations near a reference site. The reference site was selected by examination of the signal to noise on common events and site geology. Station NEOK has a category (a) geology from Table 2, and is centrally located to the stations PSAR, FILI, MAGO, ZOFR, PEFK, and COUR, with which the ratios were taken. These are UoADGG sites. Station SPLA was chosen as the reference site for stations FIXA, ATHA, ATHB, DEKL, DMKA, and SGMA. There are no Geology category (a) sites among this cluster. SPLA was chosen as the reference site because the spectral ratio between NEOK and SPLA indicates that there is very little difference between these two sites, so that ratios in both clusters generally reflect the same relative values. This latter cluster are NOAGI stations; some of these stations recorded the main event and those ratios were also calculated for comparison. Other stations listed in Table 1 that were not used in the spectral ratios were either too far from a reference site (RFNA, THVC, and STEF) or did not have any events in common with a reference site (DFNA, PNTA, and RNTA). SGMB and SPLB are examined separately relative to nearby surface sites.

Traditionally, the basic assumption in spectral ratios is that source effects and travel paths are essentially the same for spectral ratio pairs and the ratios will primarily reflect the differences in amplification of the site geology. In this study, lateral distances from the reference site NEOK to stations PSAR, FILI, MAGO, ZOFR, PEFK, and COUR are 7.6, 8.9, 10.2, 5.7, 3.4, and 5.8 km, respectively; while hypocentral distances to individual stations range from 9 to 20.0 km, with an average distance to station NEOK of 12 km. Lateral distances from reference site SPLA, to stations FIXA, ATHA, ATHB, DMKA, DEKL, and SGMA are 4.8, 5.2, 7.8, 9.7, 12.7, and 3.4 km respectively; while hypocentral distances range from 15 to 40 km with an average distance to station SPLA of 20 km. The events used in the analysis of stations relative to NEOK tend to be beneath the stations, while events used in the analysis of stations relative to station SPLA tend to be north of the stations. The travel paths to the cluster of stations near SPLA generally satisfy the criteria of common travel paths, while the geometry of travel paths to some of the stations near NEOK do not. However, we consider the whole path in this case to be part of the site response since the events are basally underneath the stations. Actual hypocentral distances are generally about the same for pairs of stations used. Further, it has been shown that site specific variations generally occur near the surface and not at basement depths (Steidl, 1993). This also appears to be true in this case since the variance of spectral ratios in Figs. 8 and 9 is small, even though the travel paths through the deeper geology is varied.

The two horizontal components of the full time series were used in the spectral ratios, which are primarily S-wave energy. The time series were tapered, their Fourier amplitude spectra

obtained, and the square-of-sum-squared calculated. The ratios are for spectral division with records from the site of interest divided those from the reference site. This is essentially the horizontal average spectral ratio method (Baise et al., 2002), but the horizontal components are combined because the sites are far apart enough that doing the spectral division by individual components with the same orientation does not have relevance. Figs. 8 and 9 show spectral ratios' average values (dark line) and the plus and minus standard deviation values (dashed lines) for all available recording pairs obtained at each site with respect to reference sites NEOK and SPLA, respectively. Fig. 10 shows the spectral ratios between SPLA and NEOK. Few ratios had enough pairs (listed on the ordinate axis) to get meaningful statistics on standard deviation, but the values plotted give an idea of the scatter of individual ratio estimates. Examples of time series from one of the events is also shown. Also shown in Fig. 9 is the spectral ratio obtained

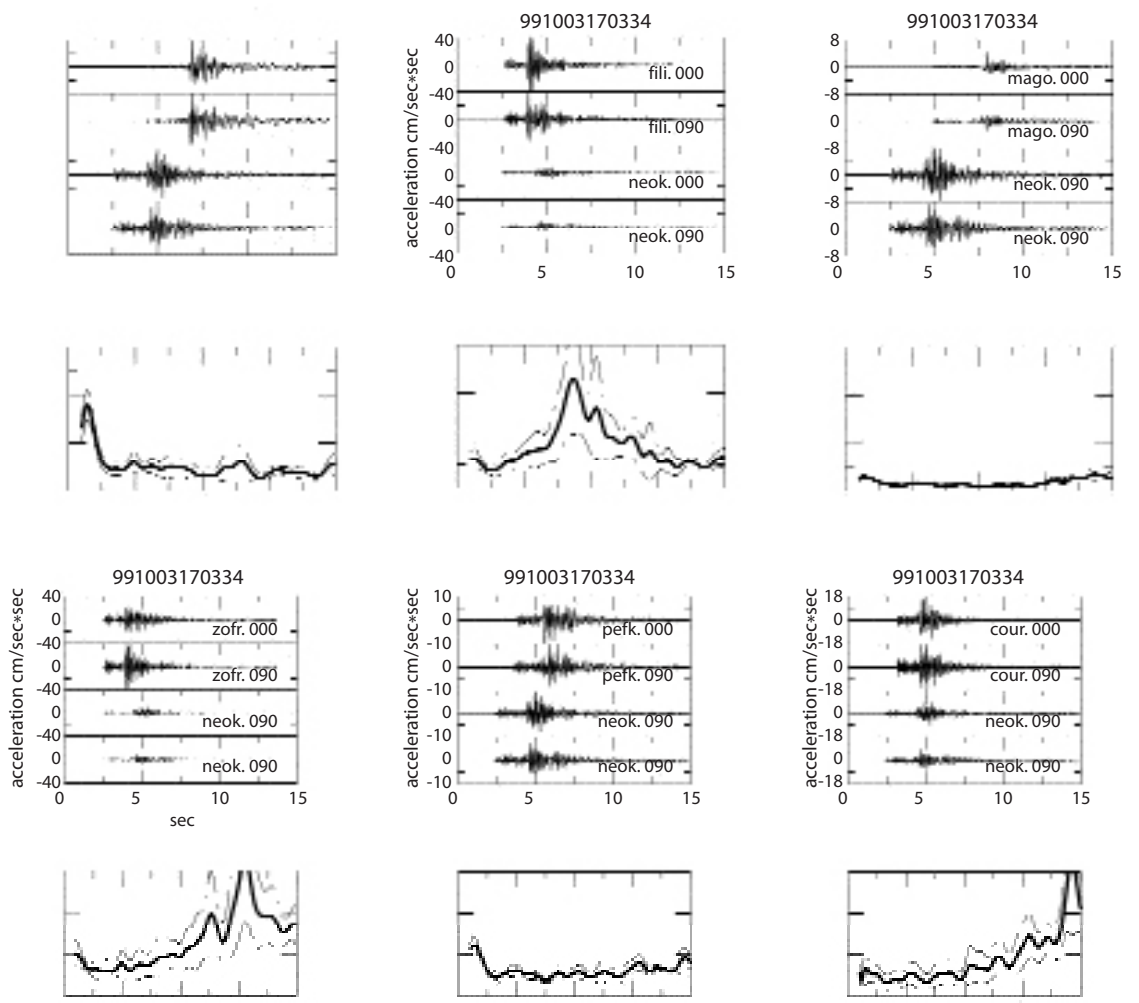

Fig. 8 - Spectral ratios with reference site NEOK for all recorded events at the station pair indicated (dark line), and the plus and minus one standard deviation values (dashed lines). The numbers of pairs used is listed on the ordinate axes. Above the ratios is an example of recordings same event for all stations.

from the main shock (dotted line) when available.

Examining Figs. 8 and 9, there is an amplification at some sites of up to about a factor of 6 at some frequencies relative to reference sites (PSAR, FILI, MAGO, ZOFR, COUR, ATHB, DEKL, and SGMA). The very high apparent amplification at low frequencies for stations ATHB and DEKL may be due to noise. Stations MAGO, FIXA, ATHA, and DMKA, SGMA show a significant de-amplification relative to the reference site of between a factor of 2 to 4 at some frequencies. Spectral ratios using the main shock show essentially the same values as those obtained with aftershocks. The main shock can have source effects on the spectra that are different at stations spaced relatively far apart (Jarpe et al., 1988), and may not provide a direct comparison to those obtained from small earthquakes. That does not appear to be the case for the four sites that had main shock recordings in this study.

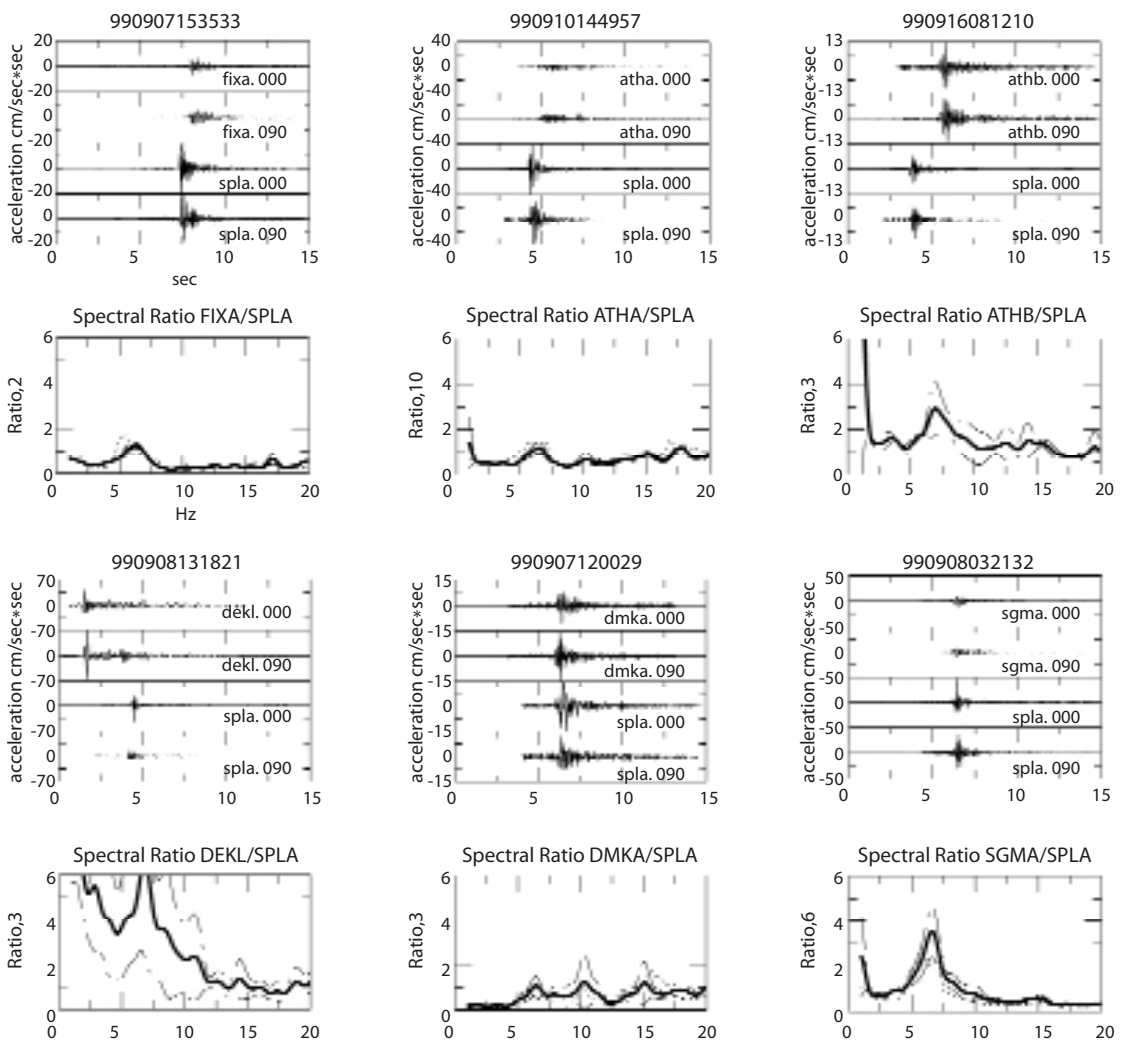

Fig. 9 - Spectral ratios with reference site SPLA for all recorded events at the station pair indicated. Spectra ratios obtained from the main event are plotted with a dotted line. The numbers of pairs used is listed on the ordinate axes. Above the ratios is an example of recordings several different events used.

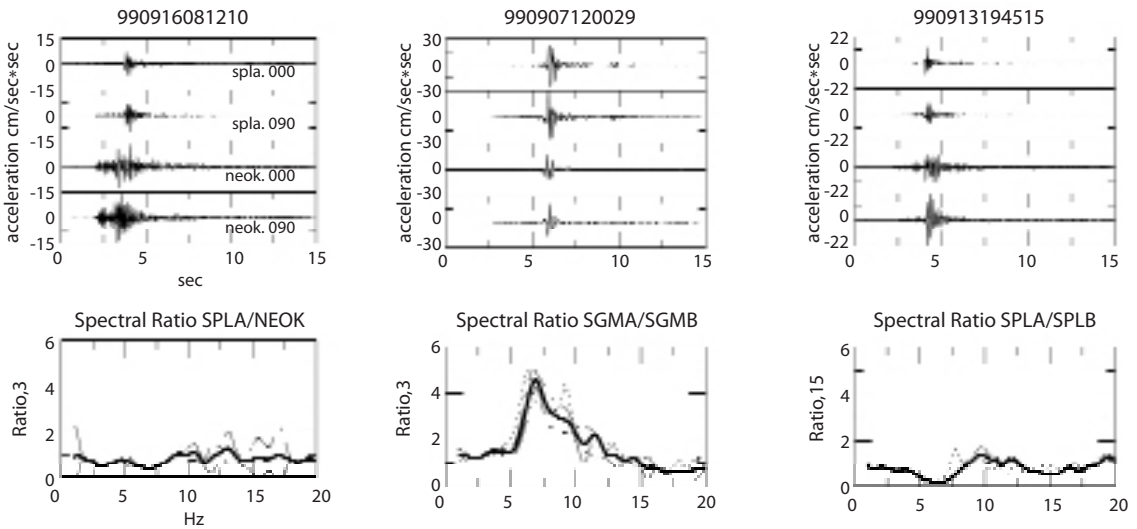

Fig. 10 - Spectral ratios for the two reference sites SPLA/NEOK, and spectral ratios of the two surface and deeper recording pairs: SPLA/SPLB and SGMA/SGMB. The numbers of pairs used is listed on the ordinate axes. SPLA is 150 m distant laterally from SPLB.

Two locations had two recorders at different vertical positions. Examining spectral ratios at these sites gives some insight into the effect of differences in near-surface materials. Fig. 10 shows spectral ratios of the two pairs: SGMA/SGMB and SPLA/SPLB. SGMA and SGMB are -7 and -26 m deep, respectively, and at a horizontal spread of about 50 m. We observe an amplification of energy in the range of 5 to 8 Hz, peaking around 7 Hz for this pair. The most recent sedimentary layers could be causing the observed amplification. SPLA and SPLB are -13 m and at the surface site, respectively, and at a horizontal spread of about 150 m. SPLB is located in the basement of a 3-story steel structure. There is no significant amplification observed in the spectral ratio of these stations. Finally, we do not observe a spectral hole for the deeper stations SPLA and SGMB, possibly because the depth difference is too little for a spectral hole to be observed in the recorded frequency range (Baise et. al., 2002).

7. Analysis and discussion

We examine the relation among t^*, spectral ratios, geologic site conditions and intensity. Our primary goal is to identify the best approach to predict potential damage from large earthquakes. We use the individual station intensity values listed in Table 2 in the analysis. In the analysis we hypothesize low t_g^* as being associated with very competent category (a) geology and little damage; intermediate values as being associated with category (b) type geology and moderate damage; and high values as being associated with poorly consolidated geology (category c) and high damage. Table 2 outlines the site specific geology and lists categories; categorization is discussed in the text. Spectral ratios used are shown in Figs. 8 and 9.

Examining these relationships is inherently qualitative. For example, the wavelengths

for which t_g^* is calculated are in the order of 100 m to 1000 m and it is not clear if the surface geology extends to these depths. Also, spectral ratios are typically very sensitive to near-surface geology, so they are not necessarily sampling the same geology as t_g^*. However, arrivals used in spectral ratios also include the effects of deeper geology, so they may represent a combination of surface geology and deeper geologic structure.

Relative intensity values depend upon distance to the hypocenter and source rupture effects as well as geologic conditions. However, even the hypocenter of this earthquake is constrained to only within about 10 km (Ioannidou et al., 2002). We use the hypocenter determined from Papadopoulos et al. (2000) and list distances to stations in Table 2. With the exception of THVC and RFNA, it is apparent from Table 2 that there is very little correlation between distances and intensity values. We hypothesize that for most of these sites the distances to the hypocenter are essentially equal as far as geometrical spreading, whole path attenuation, and the wavelengths for strong ground motions are concerned. Ioannidou et. al. (2002) have shown that there is little source directivity effects on the strong ground motion so that source rupture effects are not considered a major factor in the intensity distribution either. Another factor supporting this is the fact that many stations are located close to one another, so that source effects will be about the same for many of the stations.

Four sites had intensity VIII: FILI, ZOFR, COUR, and DEKL. These four sites have the highest amplifications of the spectral ratios computed of up to about a factor of 5 to 8 at particular frequencies. These sites have t_g^* values of 0.0034, 0.0026, 0.0027, and 0.0271, respectively. The site geology are categories are (b), (a), (a), and (c), respectively. From this we conclude that the spectral ratios correlate with damage and t_g^* values and site geologies do not since they show no consistent value that might be associated with damage. t_g^* values correlate with geology as the two category (a) sites have the lowest values, the category (b) site has a higher value, and the category (c) sites is significancy higher than the others. The spectral ratios do not correlate with surface geology as they might suggest unconsolidated (category c) geology. From this we conclude that spectral ratios are the best indicator of damage from large earthquakes.

The spectral ratio results are in agreement with the fact that both COUR and ZOFR are based on the same Permian formation and locations have similar tectonic deformation. Amplification in both stations is probably due to the fact that NEOK is based on pure limestone of possible greater thickness. COUR site amplifies frequencies above 13 Hz. The site of FILI shows significant amplification at frequencies 7-13 Hz which is attributed to the local geological conditions of the non-carbonate members of the Permian formation.

Seven sites had intensity VII: PEFK, SPLA, SPLB, PSAR, MAGO, STEF, and NEOK. They have t_g^* values of 0.0037, 0.0053, 0.0046, 0.0166, 0.0056, 0.0111, 0.0024, respectively. They have geology categories (c), (c), (c), (c), (a), (b), and (a), respectively. None of the sites show a significant spectral ratio amplification above the reference sites. Site PSAR shows some amplification at around 1 Hz, and there was no spectral ratio for STEF. Site MAGO shows a deamplification relative to the reference sites. Since the reference sites, SPLA and NEOK, also have intensity VII values, this suggests that sites PEFK, SPLA, SPLB, and NEOK are consistent with intensity/damage estimates. FIXA and MAGO are not consistent with the others, and it is

uncertain whether PSAR and STEF are consistent. All the sites have consistent t_g^* with moderate damage, showing relatively high values, except at sites PEFK and NEOK. The geology is consistent with t_g^* values except at sites PEFK and MAGO, and with spectral ratios except at sites MAGO and NEOK. All the sites have a geology category consistent with relatively high damage except at MAGO and NEOK. From this we conclude that spectral ratios, t_g^* values, and site geology are all mostly consistent with predicting relatively high damage, and are mostly consistent with each other.

From the spectra ratios PSAR and PEFK show some amplification in low frequencies up to 2.5 Hz, peaking at 1.8 Hz due to the thick Quaternary sediments, which are thicker in PSAR. The MAGO site is also situated on limestone formation which is less fragmented and has thicker stratification and exhibits a spectral ratio of 0.5. When PSAR spectrum is compared to MAGO similar amplification in low frequencies is observed, but the ratio is greater for the whole spectrum. When PEFK is compared to MAGO amplification by a factor of 5 to 6 is present and peaks to a factor of 9 at around 10 Hz. STEF is a site similar to MAGO. Energy is amplified around 6 Hz and 15 Hz for the SPLB site with respect to reference site NEOK.

FIXA had intensity VI. Spectra ratios show a deamplification relative to the reference site SPLA, which is consistent with lower intensity than sites with intensity VII. Site FIXA has a t_g^* value 0.0046, and a category (c) geology, which are more consistent with sites that had intensity VII.

Nine sites had intensity V: ATHA, ATHB, DFNA, DMKA, PNTA, RFNA, SGMA, SGMB, and THVC. They have t_g^* values of 0.0031, 0.0025, 0.0086, 0.0024, 0.0067, 0.0048, 0.0051, 0.0076, respectively. They have geology categories (c), (c), (c), (b), (c), (b), (b). and (b), respectively. Sites DFNA, PNTA, and RFNA only have data from the main event; their spectral ratios were not computed, and their t_g^* values are only from the main event. Site THVC is too distant to get a spectral ratio. Sites ATHA, DMKA, and SGMB (not shown) all have a de-amplification of spectral ratio relative to the reference site at almost all frequencies. Sites ATHB and SGMA show a significant amplification at some frequencies. This suggests that the former are consistent with a lower intensity values and the latter are not. All the sites are a category (c) geology, which is inconsistent with lower intensity values. Sites ATHA, ATHB, DMKA, RFNA, and THVC have t_g^* that are consistent with moderate damage/intensity, while sites DFNA, PNTA, SGMA, and SGMB do not. The spectral ratios, t_g^* values, and geology are not consistent with each other. From all this we conclude that the surface geology is a poor indicator of where damage may not occur, and t_g^* and spectral ratios perform moderately well.

8. Conclusions

The aim of this study has been to evaluate whether site specific t^* (t_g^*), spectral ratios, or surface geology are decisive elements in predicting damage from strong ground motion. We used the 1999 Athens earthquake aftershock data recorded from a temporary network and data from aftershocks and the main event recorded by a permanent strong motion array in the evaluation. We conclude that the spectral ratio method is the best indicator of potential damage.

The four sites that had the highest intensities showed the highest amplifications by the spectral ratio method, and most other sites showed relative amplifications consistent with intensity. t_g^* is a moderately effective method of identifying relative amplification, but did not identify the highest intensity area. Near-surface site geology showed very poor correlation with potential damage. Spectral ratios and t_g^* did not correlate with geology very well, but show significant correlation with each other. Microzonation mapping may be better served by mapping spectral ratios and t_g^* rather than surface geology to map potential hazard.

Acknowledgments. We benefited from reviews by prof. K. Pitilakis and prof. J. Zahradnik. We also benefited from discussions with Paul Kasameyer and William Foxall. This project was partially funded by the National Observatory of Athens, Greece, which also contributed significant data and data processing. The University of Athens, Greece contributed significant computational facilities and data. This project was partially supported by the Lawrence Livermore National Laboratory, Campus/Laboratory Collaboration Project, and under the auspices of the U.S. Department of energy by the University of California, under contract No. W-7405-Eng-48. It was partially funded by Caltrans under contract #59A0238 for site response analysis.

References

Aki K.; 1969: *Analysis of the seismic coda of local earthquakes as scattered waves*. J. Geophys. Res. **74**, 615-631.

Aki K. and Richards P.G.; 1980: *Quantitative seismology. Theory and Methods. Volumes I and II*. W. H. Freeman and Company, San Francisco, CA.

Anagnostopoulosa S.A., Theodoulidis N.P., Lekids B.A. and Margaris B.N.; 1986: *Kalamata earthquake Sep. 13, 1986*. Research Rep. 86-06. Institute of Engineering Seismology and Earthquake Engineering (ITSAK), Thessaloniki.

Anderson J.G. and Hough S.; 1984: *A model for the shape of the Fourier amplitude spectra of accelerograms at high frequencies*. Bull. Seis. Soc. Am., **74**, 1969-1994.

Andrews D.J.; 1986: *Objective determination of source parameters and similarity of earthquakes of different size*. In: Das S., Boatwright J., Scholz C.H. (eds), Earthquake Source Mechanics, American Geophysical Union, Washington, D.C., pp. 259-267.

Attiko Metro; 1999: Internal Geotechnical Report, personal communication with Ioannis Kalogeras.

Baise L.G. and Glaser S.D.; 2000: *Consistency of ground-motion estimates made using system identification*. Bull. Seis. Soc. Am., **90**, 993-1009.

Baise L., Hutchings L. and Glaser S.; 2001: *Analysis of site response at Yerba Buena Island, San Francisco Bay, California from weak motion recordings*. Boll. Geof. Teor. Appl., **42**, 221-246.

Basili M. and Brady G.; 1978: *Low frequency filtering and the selection of limits for accelerogram corrections*. In: Proc. of VI European Conference on Earthquake Engineering, Sep 18-22, Dubrovnik, Yugoslavia, pp. 251-258.

Blakeslee S. and Malin P.; 1991: *High-frequency site effects at two Parkfield downhole and surface stations*. Bull. Seis. Soc. Am., **81**, 332-345.

Bonilla L.F., Steidl J.H., Lindley G.T., Tumarkin A.G. and Archuleta R.J.; 1997: *Site amplification in the San Fernando valley, CA: variability of the site effect estimation using the S-wave coda, and H/V methods*. Bull. Seis. Soc. Am., **87**, 710-730.

Borcherdt R.D.; 1970: *Effects of local geology on ground motion near San Francisco Bay.* Bull. Seis. Soc. Am., **60**, 29-61.

Bouckovalas G.D., Kouretzis G. and Kalogeras I.S.; 2002: *Site-specific analysis of strong motion data from the September 7, 1999 Athens, Greece earthquake*. Natural Hazards, **27**, 105-131.

Brune J.N.; 1971: *Tectonic stress and the spectra of seismic shear waves from earthquakes*. J. Geophys. Res., **75**, 4997-5010 (Correction, J. Geophys. Res., **76**, 5002, 1972).

Caceci M.S. and Cacheris W.P.; 1984: *Fitting curves to data: the simplex algorithm is the answer,* Byte Magazine, **9**, 340-360.

Carydis P.G., Drakopoulos J. and Taflambas J.; 1984: *Evaluation of the Corinth strong motion records of February 24 and 25, 1981*. In: Proc. 7th Europ. Conf. on Earthq. Eng., Athens, Greece.

Carydis P.G., Drakopoulos J., Kalogeras J., Mouzakis H., Taflambas J. and Vougiouka N.; 1989: *Analysis of the Kalamata, Greece, strong motion records and correlation with the observed damages*. In: Proc. of XXI General Assembly of E.S.C., Sofia, Bulgaria, pp. 344-355.

Edafomechaniki Ltd.; 1998: *Geotechnical study of the Thiva area. Ministry of Development, General Secretariat of Research and Technology,* Auto-Seismo-Geotech, Vol. B, Report 4.1.

EERI; 1999: *The Athens, Greece Earthquake of September 7, 1999. Special earthquake report - Learning from Earthquakes*. November 1999. http://www.eeri.org/earthquakes/Reconn/Greece1099/Greece1099.html.

Field E.H. and Jacob K.H.; 1993: *The theoritical response of sedimentary layers to ambient seismic noise*. Geoph. Res. Lett. **20**, 2925-2928.

Frankel A. and Wennerberg L.; 1989: *Microearthquake spectra from the Anza, California, seismic network: site response and source scaling*. Bull. Seis. Soc. Am., **79**, 581-609.

Geomechaniki Ltd; 1999: *Geotechnical report for the Planetarium Building at Evgenidis Foundation*. 10 pp.

Glaser S.D.; 1995: *System identification and its application to estimating soil properties*. J. Geotech. Eng., ASCE, **121**, 553-560.

Hartzell S.H.; 1992: *Site response estimation from earthquake data*. Bull. Seis. Soc. Am., **82**, 2308-2327.

Hashida T., Stavrakakis G. and Shimazaki K.; 1988: *Three-dimensional seismic attenuation structure beneath the Aegean region and its tectonic implication*. Tectonophysics, **145**, 43-54.

Hatzidimitriou P., Papazachos C., Kiratzi A. and Theodoulidis N.; 1993: *Estimation of attenuation structure and local earthquake magnitude based on acceleration records in Greece*. Tectonophysics, **217**, 243-254.

Hough S.E., Anderson J.G., Brune J., Vernon III F., Berger J., Fletcher J., Harr L., Hanks T. and Barker L.; 1988: *Attenuation near Anza, California,* Bull. Seis. Soc. Am., **78**, 672-691.

Hudson D.E.; 1979: *Reading and interpreting strong motion accelerograms*. EERI, Pasadena, California, 112 pp.

Hudson D.E. and Brady A.G.; 1971: *Strong motion earthquake accelerograms - Digitized & plotted data*. Vol. IIA. EERL, 71-50, California Institute of Technology, Pasadena, California.

Hutchings L.; 2002: *Program NetMoment; simultaneous calculation of moment, source corner frequency, and site specific t* from network recordings*. Lawrence Livermore National Laboratory, UCRL-ID-135693, 27 pp.

Hutchings L. and Wu F.; 1990: *Empirical Green's functions from small earthquakes - A waveform study of locally recorded aftershocks of the San Fernando earthquake*, J. Geophys. Res., **95**, 1187–1214.

Idriss I.M.; 1990: *Response of soft soils during earthquakes*. In: Duncan J.M. (ed.), H. Bolton Seed Memorial Symposium, Vol. 2, BiTech Publishers Ltd., Vancouver, B.C., Canada, pp. 273-289.

Ioannidou E., Hutchings L., Kalogeras I., Voulgaris N. and Stavrakakis G.: *Source rupture model and strong ground motion synthesis for the 7 September 1999, M=5.9 Athens Earthquake*. Bull. Seism. Soc. Am., submitted.

Jarpe S.J., Cramer C.H., Tucker B.E. and Shakel A.F.; 1988: *A comparison of observations of ground response to weak and strong ground motion at Coalinga, California,* Bull. Seism. Soc. Am., **78**, 421-435.

Jarpe S.J., Hutchings L.J., Hauk T.F. and Shakel A.F.; 1989: *Selected strong- and weak-motion data from the Loma Prieta earthquake sequence*. Seism. Res. Lett., **60**, 167-176.

Kalogeras I.S. and Stavrakakis G.N.; 1999: *Processing of the strong motion data from the September 7th, 1999 Athens earthquake*. National Observatory of Athens, Geodynamic Institute, Publ. No 10 (CD-ROM).

Katsikatsos G., Migiros G., Triandaphyllis M. and Mettos A.; 1986: *Geological structure of Internal Hellenides*. Geological and Geophysical Research Special Issue, Inst. of Geology and Mineral Exploration (IGME), Athens, Greece, pp. 191-212, (in greek).

KouskounaV., Makropoulos K., Raftopoulos D., Malakatas N., Albini P., Stucchi M. and Rubbia G.; 2000: *The September 7, 1999 Parnitha earthquake: Macroseismic observations*. Abstact in EGU, Sept. 2000, Lisbon, Portugal.

Lachet C. and Bard P.-Y.; 1994: *Numerical and theoretical investigations on the possibilities of Nakamura's technique*. J. Phys. Earth, **42**, 377-397.

Lama R.D. and Vutukuri V.S.; 1978: *Handbook on mechanical properties of rocks,* Volume II, Testing techniques and results; Trans Tech Publications, pp. 481.

Lekidis V., Pitilakis K., Margaris V., Theodoulidis N. and Moutsakis A.; 1991: *The Edessa earthquake of Dec. 21, 1991*. Institute of Engineering Seismology and Earthquake Engineering (ITSAK), Report 91-01, 68 pp.

Lekkas E.; 2001: *The Athens earthquake (7 Sept. 1999): intensity distribution and controlling factors,* Engineering Geology, **59**, 297-311.

Lermo J. and Chavez-Garcia; 1993: *Site effect evaluation using spectral ratios with only one station*. Bull. Seism. Soc. Am., **83**, 1574-1594.

Lindley G.T. and Archuleta R.J.; 1992: *Earthquake parameters and the frequency dependence of attenuation at Colinga, Mammoth Lakes, and the Santa Cruz Mountains, California*. J. Geophys. Res., **97**, 14137- 14154.

Makropoulos K., Drakopoulos J. and Kouskouna V.; 1989: *The earthquake sequence in Volos, Central Greece, April 30, 1985. Analysis of strong motion*. Abstract Book of the 25th IASPEI General Assembly, Istanbul, Turkey.

Malin P.E.; 1980: *A first-order scattering solution for modeling elastic waves codas. I. The acoustic case*. Geophys. J. R. Astr. Soc., **63**, 361-380.

Margaris V.N.; 1986: *Digitizing errors and filters*. Institute of Engineering Seismology and Earthquake Engineering (ITSAK), Report 86-03, 43 pp.

Mariolakos I. and Foundoulis I.; 2000: *The Athens earthquake Sept. 7, 1999, the neotectonic regime of the affected area*. Ann. Geol. des Pay Helleniques, Tom. XXXVIII, Fasc. B, 165-174.

Nakamura Y.; 1989: *A method for dynamic characteristics estimation of subsurface using microtremors on the ground surface*. Quart. Rev. Rail. Trans. Res. Inst. (RTRI), **30**, 25-33.

Nelder J.A. and Mead R.; 1965: *A simplex method for function minimization,* Computer J., 7, 308-313.

Papadimitriou P., Kassaras G., Voulgaris N., Kassaras I., Delibasis N. and Makropoulos K.; 2000: *The September 7, 1999 Athens earthquake sequence recorded by the Cornet Network: preliminary results of source parameters determination of the mainshock*. Ann. Geol. des Pay Helleniques, Tom. XXXVIII, Fasc. B, 29-40.

Papadopoulos G.A., Drakatos G., Papanastassiou D., Kalogeras I., Stavrakakis G.; 2000: *Preliminary results about the catastrophic earthquake of 7 September 1999 in Athens, Greece*. Seis. Res. Let., **71**, 318-329.

Papazachos C.; 1992: *Anisotropic radiation modeling of macroseismic intensities for estimation of the attenuation structure of the upper crust in Greece*. Pageoph, **138**, 445-469.

Press W.H., Flannery B.P., Teukalsky S.A. and Vetterling W.T.; 1998: *Numerical recipes*. Cambridge University Press, 933 pp.

Protonotarios I.; 1999: *Preliminary conclusions from the Sept. 9, 1999 Earthquake*. 1st Symposium in Geophysics and Seismology, Workshop on the Sept. 9, 1999 Athens Earthquake, November 2-3, 1999, Dept. of Geophysics, Univ. of Athens, Greece.

Public Works Research Center (PWRC); 1981: *A geotechnical study for a municipal building at Ag. Ioannie Rentis, laboratory tests*. Internal Report pp. 5 (in greek).

Rollins K.M., Mchood M.D., Hryciw R.D. and Homolka M.; 1994: *Ground response on Treasure Island*. Strong Ground Motion, A109-A121.

Safak E.; 1997: *Models and methods to characterize site amplification from a pair of records*. Earthquake Spectra., **13**, 97-129.

Schnabel P., Seed H.B. and Lysmer J.; 1972: *SHAKE: A computer program for earthquake response analysis of horizontally layered sites*. Earthquake Engineering Center, Report No. UCB/EERC-72/12, University of California, Berkeley.

Seed R.B., Dickson S.E. and Idriss I.M.; 1991: *Principal geotechnical aspects of the 1989 Loma Prieta earthquake*. Soils and Foundations, **31**, 1-26.

Stavrakakis G.N., Kalogeras I.S. and Drakopoulos J.C.; 1993: *Preliminary analysis of Greek accelerograms recorded at stations of NOA's network: Time period 1973 - 1990*. In: Proc. 2nd Congress Hellenic Geophys. Union, Florina, Greece, 5-7 May, pp. 175-191.

Steidl J.; 1993: *Variation of site response at the UCSB dense array of portable accelerometers*. Earthquake Spectra, **9**, 289-302.

Trifunac M.D. and Lee V.W.; 1973: *Routine computer processing of strong-motion accelerograms*. Earthquake Engineering Research Laboratory, EERL 73-03, California Institute of Technology, Pasadena, pp. 360.

Trifunac M.D. and Lee V.W.; 1979: *Automatic digitalization and processing of strong-motion accelerograms*. Part I. Univ. Southern California, Tech. rep. CE, pp. 79-151.

Trifunac M.D., Udwadia F.E. and Brady A.G.; 1973: *Analysis of errors in digitized strong-motion accelerograms*. Bull. Seism. Soc. Am., **63**, 157-187.

Tsamis; 1999: *Study for the development and extension of the building of the Nuclear Technology and Radiation Protection Institute*. Technical Report, Nuclear Center for Scientific Research "Demokritos", Athens, Greece (in greek).

Tselentis G.A. and Zahradnik J.; 1999: *Aftershock monitoring of the Athens earthquake of 7 September 1999*. Seis. Res. Let., **71**, 330-337.

Tumarkin A.G. and Archuleta R.J.; 1997: *Recent advances in prediction and processing of strong motions*, Natural Hazards, **15**, 199-215.

Voulgaris N., Kassaras I., Papadimitriou P. and Delibasis N.; 2000: *Preliminary results of the Athens September 7, 1999 aftershock sequence*. Ann. Geol. des Pay Helleniques, Tom. XXXVIII, Fasc. B, 51-62.

Wu F.T. and Ben-Menahem A.; 1965: *Surface wave radiation pattern and source mechanism of the September 1, 1962, Iran earthquake*. J. Geoph. Res., **70**, 3943-3949.